

This article was downloaded by: [University of Tokyo]

On: 03 July 2014, At: 22:19

Publisher: Taylor & Francis

Informa Ltd Registered in England and Wales Registered Number: 1072954 Registered office: Mortimer House, 37-41 Mortimer Street, London W1T 3JH, UK



International Journal of Digital Earth

Publication details, including instructions for authors and subscription information:

<http://www.tandfonline.com/loi/tjde20>

Full polarimetric PALSAR-based land cover monitoring in Cambodia for implementation of REDD policies

Ram Avtar ^a , Wataru Takeuchi ^a & Haruo Sawada ^a

^a Institute of Industrial Science , The University of Tokyo , Tokyo , Japan

Published online: 03 Oct 2011.

To cite this article: Ram Avtar , Wataru Takeuchi & Haruo Sawada (2013) Full polarimetric PALSAR-based land cover monitoring in Cambodia for implementation of REDD policies, International Journal of Digital Earth, 6:3, 255-275, DOI: [10.1080/17538947.2011.620639](https://doi.org/10.1080/17538947.2011.620639)

To link to this article: <http://dx.doi.org/10.1080/17538947.2011.620639>

PLEASE SCROLL DOWN FOR ARTICLE

Taylor & Francis makes every effort to ensure the accuracy of all the information (the "Content") contained in the publications on our platform. However, Taylor & Francis, our agents, and our licensors make no representations or warranties whatsoever as to the accuracy, completeness, or suitability for any purpose of the Content. Any opinions and views expressed in this publication are the opinions and views of the authors, and are not the views of or endorsed by Taylor & Francis. The accuracy of the Content should not be relied upon and should be independently verified with primary sources of information. Taylor and Francis shall not be liable for any losses, actions, claims, proceedings, demands, costs, expenses, damages, and other liabilities whatsoever or howsoever caused arising directly or indirectly in connection with, in relation to or arising out of the use of the Content.

This article may be used for research, teaching, and private study purposes. Any substantial or systematic reproduction, redistribution, reselling, loan, sub-licensing, systematic supply, or distribution in any form to anyone is expressly forbidden. Terms & Conditions of access and use can be found at <http://www.tandfonline.com/page/terms-and-conditions>

Full polarimetric PALSAR-based land cover monitoring in Cambodia for implementation of REDD policies

Ram Avtar*, Wataru Takeuchi and Haruo Sawada

Institute of Industrial Science, The University of Tokyo, Tokyo, Japan

(Received 6 August 2010; final version received 31 August 2011)

Forest cover monitoring plays an important role in the implementation of climate change mitigation policies such as Kyoto protocol and Reducing Emissions from Deforestation and Forest Degradation (REDD). In this study, we have monitored land cover using the PALSAR (Phased Array type L-band Synthetic Aperture Radar) full polarimetric data based on incoherent target decomposition. Supervised classification technique has been applied on Cloude–Pottier decomposition, Freeman–Durden three component, and Yamaguchi four component decomposition for accurate mapping of different types of land cover classes. Based on confusion matrix derived from the predicted and defined pixels, the evergreen and sparsely deciduous forests have shown high producer's accuracy by Freeman–Durden three component and Yamaguchi four component classifications. The overall accuracy of Maximum Likelihood Classification by Yamaguchi four component is 94.1% with 0.93 kappa coefficient as compared to the 90.3% with 0.88 kappa coefficient by Freeman–Durden three component and 89.7% with 0.88 kappa coefficient by Cloude–Pottier decomposition. High accuracy of classification in a forested area using full polarimetric PALSAR data may have been because of high penetration of L-band SAR. The content of this study could be useful for the forest cover mapping during cloudy days needed for proper implementation of REDD policies in Cambodia.

Keywords: global climate change; REDD; PALSAR; forest cover mapping

1. Introduction

Mapping of forest area is necessary for sustainable management and utilization of forest resources. Forests play an important role in terrestrial carbon flux and therefore, any significant change in the forest cover from local to global scale will affect the carbon cycle. Forest cover mapping through ground surveys is labor intensive, time consuming, relatively infrequent, very expensive, and these maps become easily outdated (Asner 2009). Development of remote sensing techniques made mapping of forest cover cost and time effective with significant accuracy. In tropical countries, the frequent cloud cover often restrains the acquisition of optical remote sensing data. Radar techniques become a feasible way of acquiring remotely sensed data within a given time frame because they are able to collect data in all weather conditions. Due to this unique feature, radar data have been used extensively in many fields, including land cover mapping (Lu 2006, Palmann *et al.* 2008).

*Corresponding author. Email: ram@iis.u-tokyo.ac.jp

Polarimetric SAR data play an important role in land cover classification (Zebker *et al.* 1991, Cloude and Pottier 1997).

In January 2006, Japan Aerospace Exploration Agency successfully launched Advanced Land Observation Satellite having L-band Synthetic Aperture Radar (SAR) sensor. Phased Array type L-band Synthetic Aperture Radar (PALSAR) full polarimetric data are advantageous to characterize various targets on the basis of physical, dielectric, and geometric properties (Ainsworth *et al.* 2009). The ability of PALSAR data to retrieve information about physical properties of the surface has led to a wide range of applications, such as monitoring of crops, hydrology, soil moisture, disaster, ocean, and forests (Lee and Pottier 2009). In this study, PALSAR data have been used for land cover classification. Co-polarized (HH, VV) and cross-polarized (HV) signals are used to determine surface scattering, double-bounce scattering, and volume scattering, respectively (Rignot *et al.* 1995). Various decomposition techniques are available for the land cover classification, however, in this study, eigen vector-based (Cloude–Pottier) and model-based (Freeman–Durden three component and Yamaguchi four component) techniques have been compared. Supervised and unsupervised classification approach using SAR data have been done by various researchers (Lee *et al.* 1999, 2004, Fang *et al.* 2006, Alberga 2007, Ainsworth *et al.* 2009). This study demonstrates the application of supervised classification on PALSAR full polarimetric data for land cover classification. The performance of supervised classification depends on the applications and the availability of ground truth data (Ince 2010).

Cloude–Pottier decomposition for polarimetric classification is based on eigen values and eigen vectors to estimate polarimetric scattering of various targets which are derived from the coherency matrix of full polarimetric PALSAR data (Cloude and Pottier 1996, 1997). Entropy (H), alpha (α), and anisotropy (A) are eigen values-based polarimetric decomposition used to understand the polarimetric response of SAR data to study purity of target, mean scattering, and number of scattering involved for each target (Lee *et al.* 2004, Patel *et al.* 2009). Freeman–Durden three component decomposition (1998) approach is the first model-based incoherent decomposition. It has been used to model the polarimetric coherence matrix as the contribution of three scattering mechanisms: surface scattering, double-bounce scattering, and volume scattering (An *et al.* 2011). The four component scattering decomposition technique proposed by Yamaguchi *et al.* (2006) which is an extension of Freeman–Durden three component decomposition has also been used in this study.

The important role of forest in the global carbon cycle has been pointed out in previous studies (Schlamadinger and Marland 1996, Brown 2002, Defries *et al.* 2007). Therefore, it becomes necessary to monitor forest covers for effective implementation of the Reducing Emissions from Deforestation and Forest Degradation (REDD) policies in a post Kyoto Protocol climate change mitigation regime. Most of the previous studies (Table 1) show the polarimetric application of SAR data using various decomposition theories. The selection of the best SAR-based decomposition classification for land cover monitoring is highly desirable in order to optimally select the appropriate methodology. Hence, a quantitative comparison between the classification results of various decomposition methods has been made in order to understand the potential of the full polarimetric PALSAR data to generate land cover map.

Table 1. Previous studies related to polarimetric decomposition.

No.	Authors	Polarimetric parameters used
1	Cloude and Pottier 1997	Entropy and Alpha-based classification
2	Lee <i>et al.</i> 1999	<i>H/A/Alpha</i> Wishart classification
3	Ferro-Famil <i>et al.</i> 2001	<i>H/A/Alpha</i> Wishart classification
4	Fang and Wen 2005	Intensity, Alpha, and Entropy
5	Ouarzeddine <i>et al.</i> 2005	Entropy, Alpha, and Anisotropy
6	Fang <i>et al.</i> 2006	Entropy, Alpha, and Span
7	Alberga 2007	Entropy, Alpha, and Anisotropy-based land cover classification
8	Patel <i>et al.</i> 2009	Entropy, Alpha, and Anisotropy
9	Wang <i>et al.</i> 2009	Krogagger decomposition with <i>T</i> matrix
10	Ince 2010	Dynamic clustering of entropy, alpha, and Anisotropy
11	An <i>et al.</i> 2011	Four component decomposition with deorientation
12	Singh <i>et al.</i> 2011	Four component scattering power decomposition

2. Study area

Cambodia has an area of 181,035 Km² in the southwestern corner of Indo-China countries, bordered with Vietnam to the east, Thailand to the west, Lao P.D.R. to the north, and Gulf of Thailand to the south. Cambodia's average temperature ranges from 21° to 35°C. The country experiences the rainy season during May to October and a dry season during November to April. The mean annual precipitation is 150–180 cm; with most precipitation occurring in mountainous regions (UNEP 2009). Cambodia has the highest rate of deforestation among Indo-China countries (FRA 2010). Between 2000 and 2005, the country lost 29% of its primary forests, while overall deforestation was 218,800 ha of forest per year (FAO 2005). Logging activities combined with rapid development, population growth, urbanization, and agricultural expansion have been the primary reasons for Cambodia's forest loss (Gaughan *et al.* 2009, UNEP 2009). Cambodia has signed REDD policies in 2009 and study of forest cover is necessary for the REDD policies implementation. The study area is situated in parts of Stung Treng and Kratie province of Northern Cambodia and covers an area of about 1852 Km² (Figure 1). Field visits were made in December 2009 and January 2011 for the collection of ground truth data. The GPS positions and GPS photos of various land cover types were collected to use as training data for supervised classification of the remote sensing data.

2.1. Land cover map of the study area

Land cover classification is useful for effective management of land resources and remote sensing technique plays an essential role for land and use land cover classification (Garcia-Mora *et al.* 2011). Forests are considered to have high biodiversity and commercial importance and play a significant role in social, economic, and cultural development of rural people (Kummer and Turner 1994). Land cover map (Figure 2) was generated using the maximum likelihood classification (MLC) technique. AVNIR-2 data acquired on March 2010 was used to generate land cover map of the area supported with ground truth data. The study area was classified into seven land cover classes viz. evergreen forest, deciduous forest, sparsely

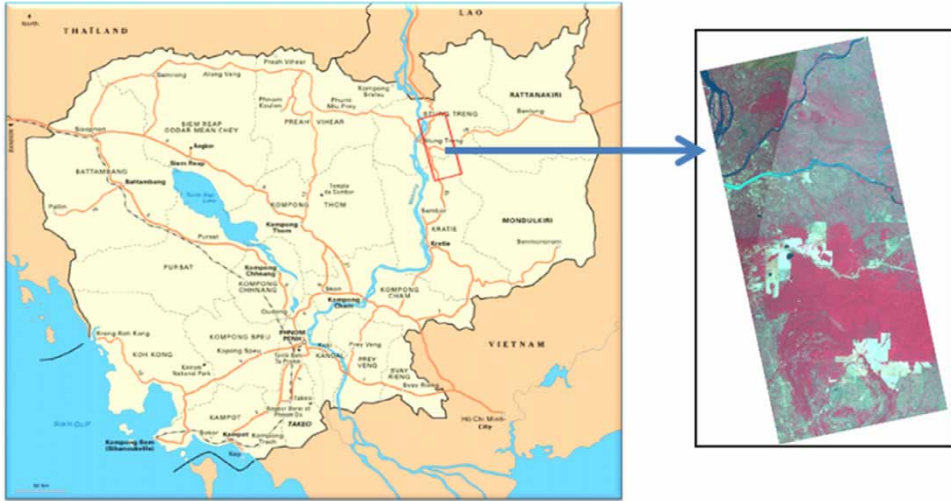


Figure 1. Location of the study area.

deciduous forest, wood and shrub land, deforested area, agricultural land, and water. It was found that most of the area is covered by evergreen forest followed by deciduous forest, sparsely deciduous forest, and other classes. Table 2 shows the percentage of different land cover classes of the area.

3. Methodology

PALSAR 1.1 level full polarimetric, single look complex (SLC) data acquired on 6 April 2009 with 21.5° look angle was used as the primary data. PolSARpro4.2 software was used for the data processing. First, the data were multi-looked one time in range and six times in azimuth and converted from slant to ground range, so that the spatial resolution would be reduced to nearly $23 \text{ m} \times 21 \text{ m}$ per pixel (range \times azimuth). Then the data were processed with the refined Lee filter with window size 5×5 to reduce the speckle noise (Lee *et al.* 2008, 2009). The detailed methodology is shown in the flow chart (Pottier *et al.* 2008)(Figure 3).

3.1. Polarimetric decompositions

Polarimetric decomposition provides information about scattering mechanisms or polarimetric properties of the targets. The decomposition method depends on the target types and is divided into two major categories: (1) coherent decomposition (pure targets) and (2) incoherent decomposition (distributed targets). Most of the objects in the study area are natural vegetation, therefore, incoherent target decomposition models were used. The incoherent target decomposition models such as Cloude and Pottier (1997), Freeman–Durden three component (1998), and Yamaguchi four component scattering model (2006) were used in this study. These models can be summarized as follows: the coherency matrix is given as

$$[T] = k.k^{*T} \quad (1)$$

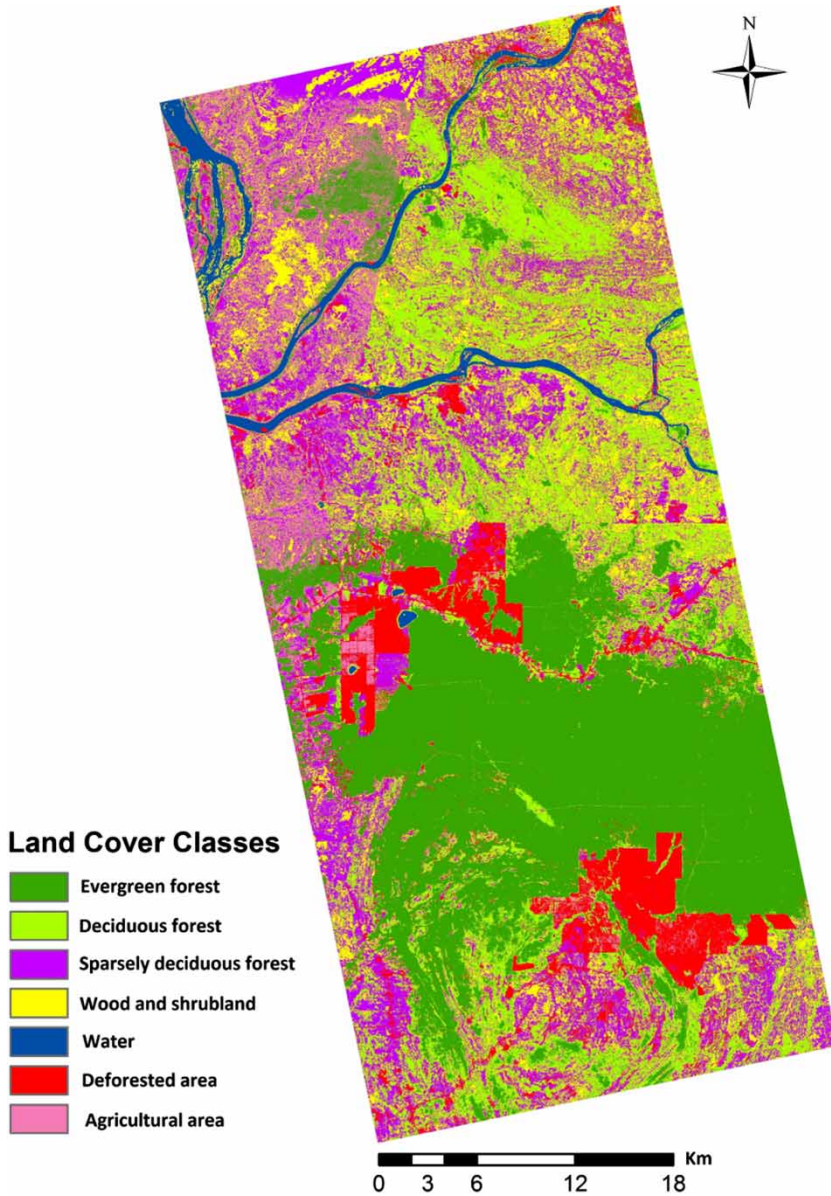


Figure 2. Land cover of the study area.

where, $*^T$ indicates complex conjugate and transpose, and k indicates the target vector.

Target vector is obtained by vectorization $V(\cdot)$ of the scattering matrix S in each pixel:

$$k = V(s) = (1/2)\text{Trace}\{S[\Psi]\} \quad (2)$$

Ψ is a set of 2 by 2 complex basis matrices.

Table 2. Percentage of different types of land cover.

Land cover classes	AVNIR-2-based classes		Cloude-Pottier-based classes		Freeman–Durden three component-based classes		Yamaguchi four component-based classes	
	Area (Km ²)	% of land cover	Area (Km ²)	% of land cover	Area (Km ²)	% of land cover	Area (Km ²)	% of land cover
Evergreen forest	550.1	29.7	637.4	34.40	808.4	43.6	617.9	33.4
Deciduous forest	388.1	21.0	477.9	25.80	264.5	14.3	391.1	21.1
Sparsely deciduous forest	387.8	20.9	232.6	12.60	309.6	16.7	456.5	24.6
Wood and shrub land	245.3	13.2	261.9	14.14	233.8	12.6	176.7	9.5
Water body	38.4	2.1	62.8	3.39	66.1	3.6	26.4	1.4
Deforested area	161.0	8.7	95.1	5.13	56.5	3.1	55.3	3.0
Agricultural land	81.4	4.4	84.4	4.56	113.2	6.1	128.2	6.9
Total	1852.1	100	1852.1	100	1852.1	100	1852.1	100

Phased Array type L-band Synthetic Aperture Radar data having monostatic mode, so target vector based on Pauli basis matrix is defined as

$$k = (1/\sqrt{2}) \begin{bmatrix} S_{hh} & + & S_{vv} \\ S_{hh} & - & S_{vv} \\ 2S_{hv} & & \end{bmatrix} \quad (3)$$

where, S_{hh} , S_{vv} , and S_{hv} are the elements of scattering matrix S .

Using Equations (1) and (3), coherency matrix $[T]$ can be written as

$$[T] = (1/2) \times \begin{bmatrix} \langle |S_{hh} + S_{vv}|^2 \rangle & \langle (S_{hh} + S_w)(S_{hh} - S_w)^* \rangle & 2\langle (S_{hh} + S_w)S_{hv}^* \rangle \\ \langle (S_{hh} - S_{vv})(S_{hh} + S_{vv})^* \rangle & \langle |S_{hh} - S_w|^2 \rangle & 2\langle (S_{hh} - S_w)S_{hv}^* \rangle \\ 2\langle S_{hv}(S_{hh} + S_w) \rangle & 2\langle S_{hv}(S_{hh} - S_w)^* \rangle & 4\langle |S_{hv}|^2 \rangle \end{bmatrix} \quad (4)$$

The incoherent decomposition theorems can be expressed as

$$[T] = q_1[T_1] + q_2[T_2] + q_3[T_3] + \dots + q_k[T_k] \quad (5)$$

This is a very general expression of incoherent decomposition where, $(q_1, q_2, q_3, \dots, q_k)$ are coefficient to be determined and $(T_1, T_2, T_3, \dots, T_k)$ expansion coherency matrix.

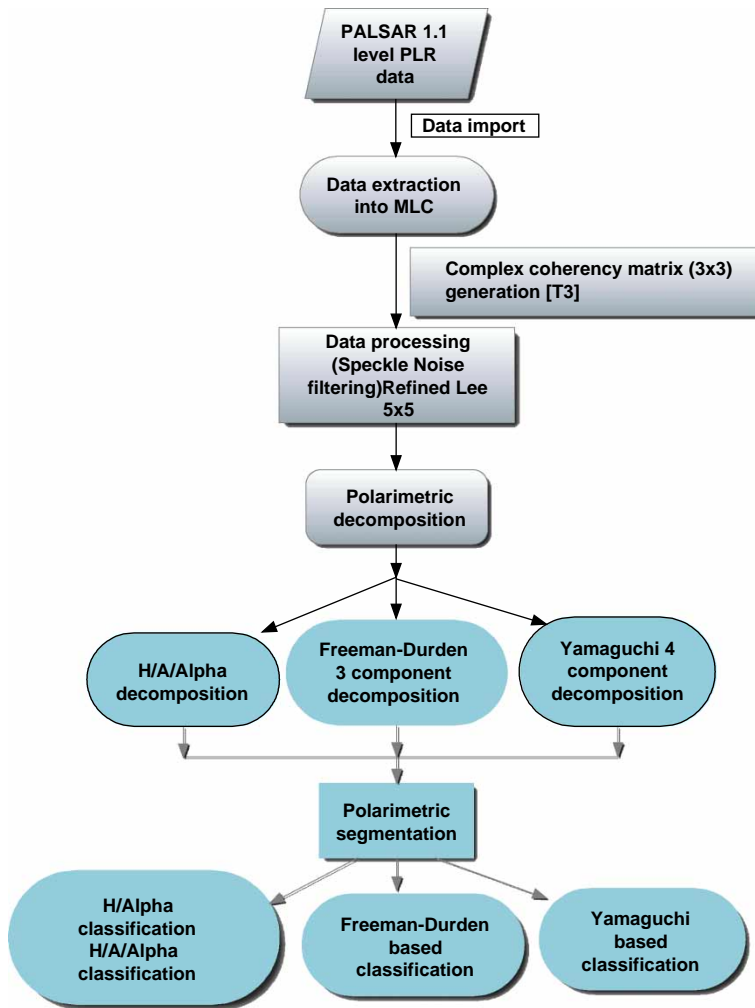


Figure 3. Flow chart of the methodology adopted for polarimetric classification.

3.2. Cloude–Pottier decomposition

Cloude and Pottier (1997) proposed a method of extraction of mean diffusion based on eigen values/eigen vectors decomposition of coherency matrix. Based on this idea, they defined entropy (H), alpha angle (α), and anisotropy (A). H , α , and A are polarimetric features that give information about scattering properties from the targets. Entropy indicates the statistical disorder (randomness) of the scatterers. Zero (0) value of H indicates a single scattering mechanism, whereas 1 indicates a random mixture of scattering mechanism (no dominant scatterers). H can be expressed as

$$H = \sum_{i=1}^3 -P_i \log_3 P_i \quad (6)$$

$$0 \leq P_i = \frac{\lambda_i}{\sum_{i=1}^3 \lambda_i} \leq 1 \quad (7)$$

where P_i is pseudo-probabilities, which can be obtained from the eigen values λ_i , represent relative intensity of the i -th scattering process.

The alpha angle (α) is estimated from α_i angle of each of the eigen vectors as follows:

$$\bar{\alpha} = \sum_{i=1}^3 P_i \alpha_i \quad (8)$$

α angle is based on the eigen vectors and is a number indicative of the average or dominant scattering mechanism within a specific target. It varies between 0° and 90° . The value of α close to 0° represents odd-bounce scattering from flat surfaces, close to 45° represents dipole or volume scattering, while a value of α close to 90° represents a double-bounce scattering.

Anisotropy (A) is a complementary parameter for entropy (H). Anisotropy measure relative importance of the second and third eigen values of eigen decomposition. It has less information than H/α and it is useful when $H > 0.7$ (Pottier 1998, Fang *et al.* 2006, Trisasongko 2010).

$$A = \frac{\lambda_2 - \lambda_3}{\lambda_2 + \lambda_3} \quad (9)$$

where, λ_2 and λ_3 are smaller eigen values.

3.3. Target decomposition theorem of Freeman and Durden (1998)

The three component scattering decomposition is a technique used for the fitting of a physically based three component scattering mechanism model to the polarimetric SAR data. Freeman–Durden decomposition is used to derive meaningful information about scatterers characteristics (i.e. volume, odd, and double-bounce scattering). This approach can be used to determine the first order dominant scattering mechanism that gives rise to observed backscatter in polarimetric SAR image. According to three components scattering decomposition techniques, the coherency matrix can be decomposed into

$$[T] = f_s[T_s] + f_d[T_d] + f_v[T_v] \quad (10)$$

Surface scattering is the first component of three scattering decomposition generated by Bragg surface scatterer

$$[T_s] = f_s \begin{bmatrix} \langle |\eta + 1|^2 \rangle & \langle (\eta + 1)(\eta - 1)^* \rangle & 0 \\ \langle (\eta + 1)^* (\eta - 1) \rangle & \langle |\eta + 1|^2 \rangle & 0 \\ 0 & 0 & 0 \end{bmatrix} \quad (11)$$

In Equations (10) and (11),

$$f_s = |R_{vv}|^2 \quad \text{and} \quad \eta = \frac{R_{hh}}{R_{vv}} \tag{12}$$

$$R_{hh} = \frac{\cos \theta - \sqrt{\epsilon_s - \sin^2 \theta}}{\cos \theta + \sqrt{\epsilon_s - \sin^2 \theta}} \tag{13}$$

$$R_{vv} = (\epsilon_s - 1) \frac{\sin^2 \theta - \epsilon_s (1 + \sin^2 \theta)}{\left[\epsilon_s \cos \theta + \sqrt{\epsilon_s - \sin^2 \theta} \right]^2} \tag{14}$$

Double-bounce scattering is modeled by scattering from a dihedral corner reflector, such as ground-tree trunk backscatter, where the reflector surfaces can be made of different dielectric materials. The coherency matrix for double-bounce scattering is represented by

$$[T_d] = f_d \begin{bmatrix} \langle |\chi - 1|^2 \rangle & \langle (\chi - 1)(\chi + 1)^* \rangle & 0 \\ \langle (\chi - 1)^* (\chi + 1) \rangle & \langle |\chi + 1|^2 \rangle & 0 \\ 0 & 0 & 0 \end{bmatrix} \tag{15}$$

where,

$$f_d = |R_{Tv}R_{Gv}|^2 \quad \text{and} \quad \chi = \frac{R_{hh}}{R_{vv}} \tag{16}$$

where, R_T and R_G are reflection coefficient of vertical trunk surface and Fresnel reflection coefficient of horizontal ground surface.

The volume scattering component is a third scattering component of the decomposition model and can be represented by

$$[T_v] = \frac{f_v}{3} \begin{bmatrix} 4 & 0 & 0 \\ 0 & 2 & 0 \\ 0 & 0 & 2 \end{bmatrix} \tag{17}$$

3.4. Target decomposition theorem of Yamaguchi et al. (2006)

Based on the Freeman–Durden three component scattering model, Yamaguchi *et al.* (2006) proposed a four component scattering decomposition technique by introducing helical scattering. This helix scattering power term, corresponds to $\langle S_{HH}S^*_{HV} \rangle \neq 0$ and $\langle S_{HV}S^*_{VV} \rangle \neq 0$ appears in heterogeneous areas (complicated shape targets or man-made structures) whereas it disappears for almost all natural distributed scattering (Yamaguchi *et al.* 2005). The coherency matrix can be decomposed into

$$[T] = f_s [T_s] + f_d [T_d] + f_v [T_v] + f_c [T_c] \tag{18}$$

where f_s , f_d , f_v and f_c are coefficients to be determined. $[T_s]$, $[T_d]$, $[T_v]$, and $[T_c]$ are expansion coherency matrix corresponding to the surface, double bounce, volume, and helix scattering, respectively.

The single-bounce scattering model is represented by surface scattering properties from rough surfaces in which the cross-polarized component is negligible. The expansion coherency matrix is expressed as

$$[T_s] = f_s \begin{bmatrix} 1 & \eta^* & 0 \\ \eta & |\eta|^2 & 0 \\ 0 & 0 & 0 \end{bmatrix} \quad (19)$$

The expansion coherency matrix for double-bounce scattering is expressed as

$$[T_d] = f_d \begin{bmatrix} |\chi|^2 & \chi & 0 \\ \chi^* & 1 & 0 \\ 0 & 0 & 0 \end{bmatrix} \quad (20)$$

The helix scattering power is equivalent to circular polarization power. This expression becomes visible in urban and mountainous areas. The helix scattering expansion matrix, which takes into account of non-reflection symmetry condition, is expressed as

$$[T_c] = f_c \begin{bmatrix} 0 & 0 & 0 \\ 0 & 1 & \pm j \\ 0 & \pm j & 1 \end{bmatrix} \quad (21)$$

Most of the area in the present study is covered by forest so the helix scattering is not the main component except in mountainous area. Hence, emphasis was given to the volume scattering from the forested area.

For the volume scattering model, one of the following matrices can be selected according to the magnitude balance of $|S_{hh}|^2$ and $|S_{vv}|^2$. These equations represent the different distribution of vegetation to discriminate different types of vegetation (Yamaguchi *et al.* 2005). When $10 \log (|S_{vv}|^2/|S_{hh}|^2) \geq 2$ dB

$$[T_v] = \frac{1}{30} \begin{bmatrix} 15 & -5 & 0 \\ -5 & 7 & 0 \\ 0 & 0 & 8 \end{bmatrix} \quad (22)$$

When $10 \log (|S_{vv}|^2/|S_{hh}|^2) < 2$ dB

$$[T_v] = \frac{1}{4} \begin{bmatrix} 2 & 0 & 0 \\ 0 & 1 & 0 \\ 0 & 0 & 1 \end{bmatrix} \quad (23)$$

When $10 \log (|S_{vv}|^2/|S_{hh}|^2) \leq -2$ dB

$$[T_v] = \frac{1}{30} \begin{bmatrix} 15 & 5 & 0 \\ 5 & 7 & 0 \\ 0 & 0 & 8 \end{bmatrix} \quad (24)$$

where f_s , f_d , f_v and f_c are surface, double, volume, and helix scattering coefficients, respectively.

3.4. Classification technique

H/A /Alpha Cloude–Pottier decomposition, Freeman–Durden three component, and Yamaguchi four component scattering approaches have been attempted for the classification of PALSAR image. Supervised classification was applied on Cloude–Pottier decomposition, Freeman–Durden three component, and Yamaguchi four component decomposition. For supervised classification, we used MLC, which is a parametric classifier that assumes normal or near normal spectral distribution for each feature of interest (Lu and Wang 2004). This classifier evaluates variance and covariance when classifying an unknown pixel. Confusion matrix was used to evaluate the performance of a classifier (Kohavi and Provost 1998). Confusion matrix is a matrix plot between the predicted and defined classes. Kappa coefficient was also used to assess the accuracy of the classification (Congalton 1991).

4. Results and discussion

The polarimetric decomposition techniques were applied on the PALSAR data. The α , H , and A of the PALSAR data have been generated from eigen values-based target decomposition, shown in Figure 4a, b, and c, respectively. The value of alpha (Figure 4a) represents the spatial variation. In Figure 4a, about 60–70% of the area has shown the values of alpha between 40° and 50° because of the volume or

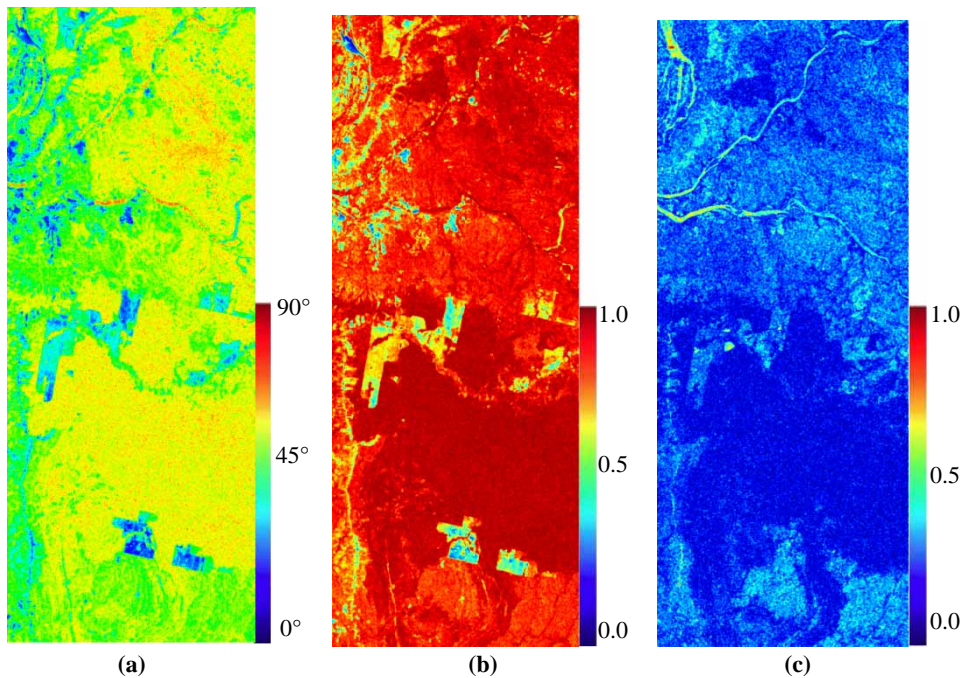


Figure 4. (a) Alpha, (b) entropy, and (c) anisotropy images of PALSAR data.

multiple scattering which is a characteristic of forests. The low value of α (10° – 20°) represents surface scattering and is a characteristic of plane surfaces such as a water body or deforested area or agricultural land. As have been stated, entropy indicates statistical disorder or randomness in the targets. Higher values of H are visible in Figure 4b which means the backscattered signals are much depolarized. This is a characteristic feature of the evergreen forest. The value of H in evergreen forest is higher than deciduous forest (Figure 4b). This indicates more randomness in evergreen forest as compared with deciduous forest. The value of H in the deforested area is lower than those in the surrounding forests. Therefore, decrease in entropy is determined as an identification of deforestation and forest degradation and is confirmed using the ground truth data. The low value of entropy and alpha in the deforested area is because of the surface scattering which causes a reflection of signal far from the sensor. The anisotropy (Figure 4c) shows most of the area having a high value of entropy which corresponds to secondary and tertiary scattering. The area with low value of entropy represents dominant first scattering and low secondary scattering.

The $H/A/\text{Alpha}$ -based R:G:B color composite image is presented in Figure 5a. In this image we can clearly differentiate the dense forest and deforested area. It gives an idea about the $H/A/\text{Alpha}$ behavior of various targets.

R:G:B color composite of Freeman–Durden three component decomposition (double bounce assigned red, volume scattering assigned green, and surface scattering assigned blue) and Yamaguchi four component decomposition images are shown in Figure 6a and 6b, respectively. It gives an approximate percentage of each of the surface, volume, and double-bounce scattering mechanisms present in the area. From Figure 6a and b, it becomes clear that volume scattering is dominant in the Freeman–Durden three component decomposition image than the Yamaguchi four component decomposition image. Most of the evergreen forest shows green color because of higher value of volume backscattering as compared with deciduous forest. In the dry season, sparse deciduous forest of the study area shows cyan color because of higher surface backscattering than volume scattering. Deforested area has high surface scattering and can be clearly distinguished from the surrounding forested area (Figure 6a and b).

MLC technique has been applied on Figure 5a and Figures 6a, and 6b with the same training samples based on field information. Classified PALSAR images using Cloude–Pottier $H/A/\text{Alpha}$ decomposition, Freeman–Durden three component, and Yamaguchi four component scattering model have been presented in Figure 5b and Figures 8a, and 8b, respectively. PALSAR data have been classified into seven major classes. Table 2 illustrates the land cover percentage obtained from the Cloude–Pottier $H/A/\text{Alpha}$ decomposition, Freeman–Durden three component, and Yamaguchi four component-based classification taking AVNIR-2 as a reference.

As given in Table 2, the areas of different land cover classes are different for each classification. The area of evergreen forest is over estimated by about 4.7%, 3.7%, and 13.9% in Cloude–Pottier classification, Yamaguchi four component, and Freeman–Durden three component classification, respectively. Freeman–Durden three component classification has shown overestimation (13.9%) in evergreen forest may be because of the over estimation problem in volume scattering component. The area of deciduous forest is 7% underestimated in Freeman–Durden classification and 4.8% overestimated in Cloude–Pottier classification, whereas Yamaguchi

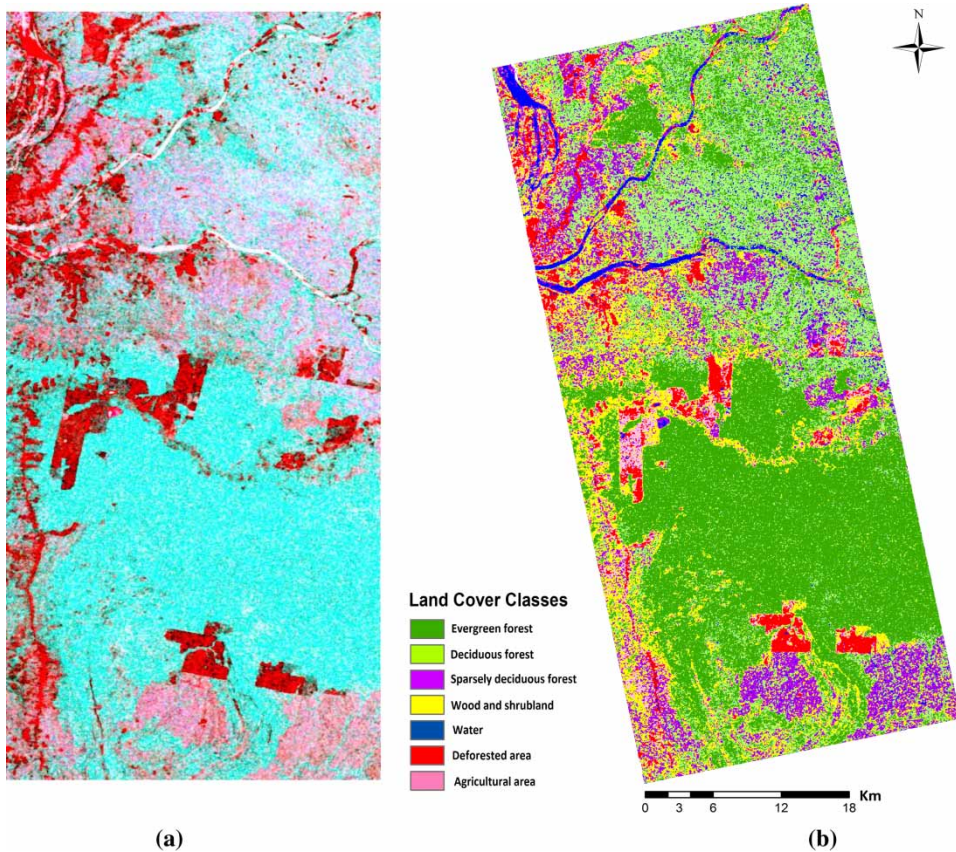


Figure 5. (a) $H/A/\text{Alpha}$ (H -Green; A -Red; Alpha -Blue) color image and (b) $H/A/\text{Alpha}$ -based land use map (MLC).

classification shows the same area. Underestimation in deciduous forest, by Freeman–Durden three component classification probably because some of the deciduous forests have shown the same volume scattering as evergreen forests did. This can be confirmed based on the field pictures (Figure 7) because deciduous forests were covered by tall grass, which causes volume scattering. Cloude–Pottier-based classification shows 8.3% underestimation in sparsely deciduous forests, which might be because of low value of alpha in sparsely deciduous forest, hence represents surface scattering behavior. Deforested area, water body, and agricultural land may have been somewhat misclassification because flat surfaces have less backscattering in L-band and cannot be distinguished easily. If agricultural land has some crops then it may be easy to distinguish from the flat surface because crop causes volume scattering.

The most common tool to access the accuracy of classification is the confusion matrix. Tables 3 and 4, and Table 5 illustrate confusion matrix of Cloude–Pottier MLC, Freeman–Durden three component MLC, and Yamaguchi four component MLC based on the predicted and defined pixels, respectively. It shows high agreement between the observed estimate and the field measurement. Therefore, it

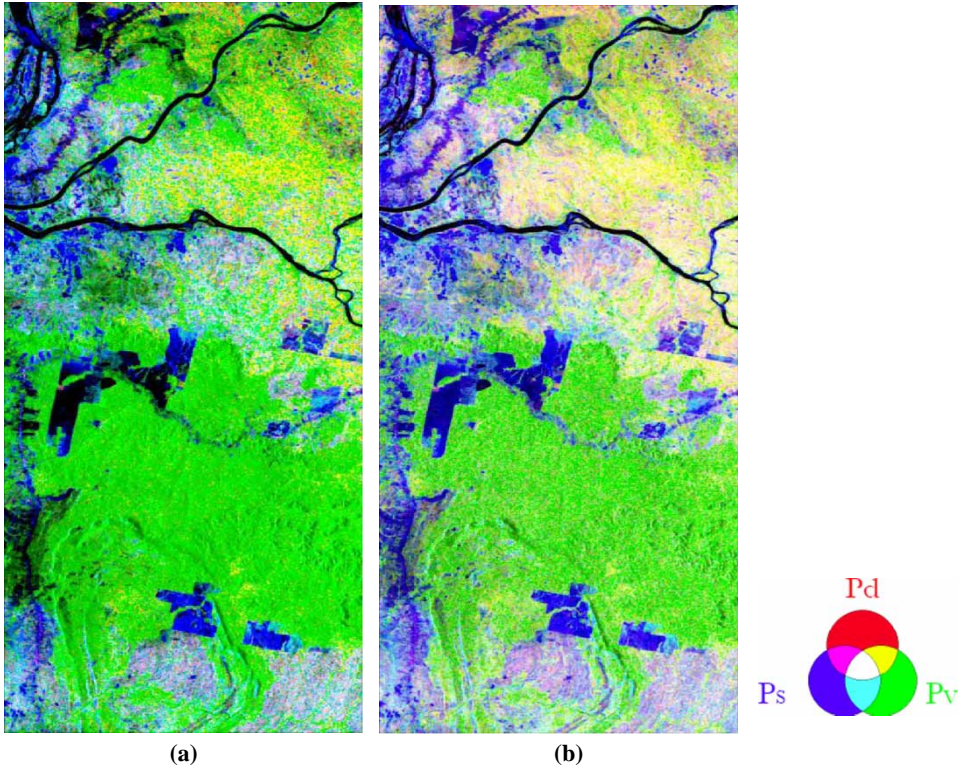


Figure 6. (a) Freeman–Durden three component-based image of PALSAR and (b) Yamaguchi four component-based image of PALSAR (R: double-bounce scattering, G: volume scattering, and B: surface scattering).



Figure 7. Deciduous forest covered by grass (> 50 cm height).

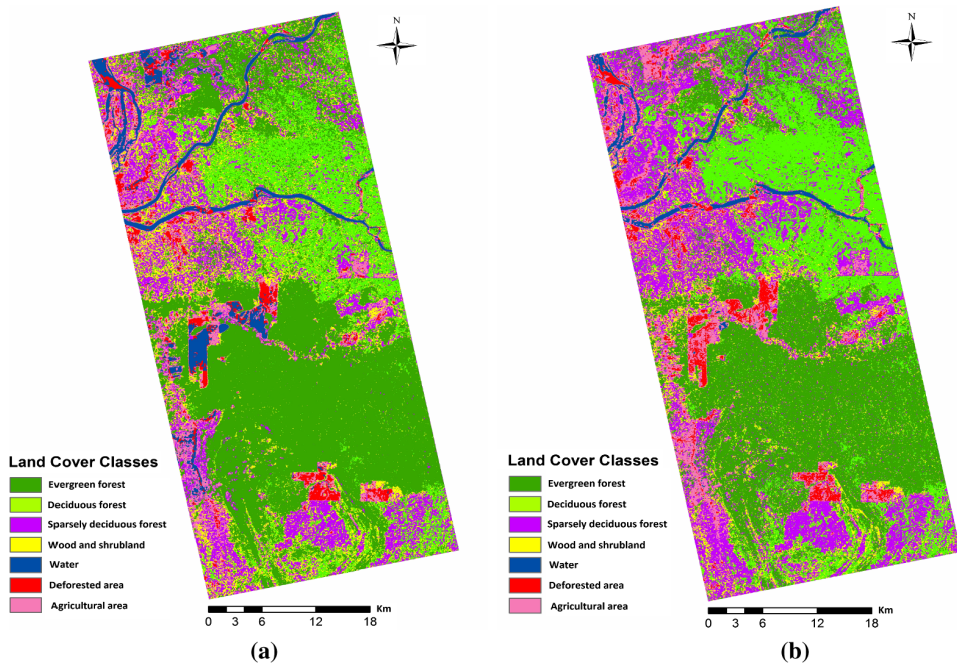


Figure 8. (a) Freeman–Durden three component-based land use map and (b) Yamaguchi four component-based land use map (MLC).

appears that field measurement is necessary to obtain precise measurement of land cover types. The evergreen and sparsely deciduous forests have shown the matrix with 100% producer's accuracy for Freeman–Durden three component and Yamaguchi four component-based classification, whereas other types of land cover have shown some variability in the matrix. Overall, Yamaguchi four component-based MLC produced highest accuracy with accuracy of 94.1% and 0.93 kappa coefficient than the 90.3% with 0.88 kappa coefficient by Freeman–Durden classification and 89.7% with 0.88 kappa coefficient by Cloude–Pottier classification (Table 6). The low accuracy of Cloude–Pottier MLC might be because of the eigen values-based decomposition, where the information associated with eigen vectors is not utilized but still it gives better accuracy.

5. Conclusion

This study demonstrates the potential of using full polarimetric L-band PALSAR data for land cover classification. Cloude–Pottier $H/A/\alpha$, Freeman–Durden three component, and Yamaguchi four component decomposition were used to study land cover in Cambodia. The evergreen and sparsely deciduous forests have shown the confusion matrix with high accuracy for both Freeman–Durden three component and Yamaguchi four component-based classification. Freeman–Durden three component classification shows overestimation in volume scattering in evergreen forest. It is interesting that overall accuracy of Yamaguchi four component-based MLC (94.1%) is more as compared with the Freeman three component-based

Table 3. Confusion matrix of Cloude–Pottier H/A/Alpha-based MLC.

	Evergreen forest	Deciduous forest	Water body	Sparsely deciduous forest	Wood and shrub land	Deforested area	Agricultural land	Total	Users accuracy
Evergreen forest	60	3	0	0	0	0	0	63	95.2%
Deciduous forest	1	43	4	1	0	0	0	49	87.7%
Water body	0	2	61	0	0	0	0	63	96.8%
Sparsely deciduous forest	0	0	5	49	2	0	1	57	85.9%
Wood and shrub land	0	1	0	1	29	1	2	34	85.3%
Deforested area	0	0	2	0	0	49	6	57	85.9%
Agricultural land	0	0	0	0	1	2	16	19	84.2%
Total	61	49	72	51	32	52	25	342	–
Producer's accuracy	98.4%	87.8%	84.7%	96.1%	90.6%	94.2%	64%	–	–

Table 4. Confusion matrix of Freeman–Durden three component-based MLC.

	Evergreen forest	Deciduous forest	Water body	Sparsely deciduous forest	Wood and shrub land	Deforested area	Agricultural land	Total	Users accuracy
Evergreen forest	61	4	0	0	1	0	0	66	92.4%
Deciduous forest	0	44	0	0	3	0	0	47	93.6%
Water body	0	0	66	0	0	7	9	82	80.5%
Sparsely deciduous forest	0	0	0	53	0	0	0	53	100%
Wood and shrub land	0	1	0	0	29	0	0	30	96.6%
Deforested area	0	0	6	0	0	44	2	52	84.6%
Agricultural land	0	0	0	0	0	0	12	12	100%
Total	61	49	72	53	33	51	23	342	–
Producer's accuracy	100%	90%	92%	100%	87%	86%	52%	–	–

Table 5. Confusion matrix of Yamaguchi four component-based MLC.

	Evergreen forest	Deciduous forest	Water body	Sparsely deciduous forest	Wood and shrub land	Deforested area	Agricultural land	Total	Users accuracy
Evergreen forest	61	0	0	0	0	0	0	61	100%
Deciduous forest	0	49	0	0	0	0	0	49	100%
Water body	0	0	64	0	0	0	0	64	100%
Sparsely deciduous forest	0	0	0	53	0	0	0	53	100%
Wood and shrub land	0	0	0	0	33	0	0	33	100%
Deforested area	0	0	8	0	0	46	7	61	75.4%
Agricultural land	0	0	0	0	0	5	16	21	76.2%
Total	61	49	72	53	33	51	23	342	–
Producer's accuracy	100%	100%	89%	100%	100%	90%	70%	–	–

Table 6. Accuracy assessment of MLC.

	Overall accuracy	Kappa coefficient
Cloude–Pottier-based classification	89.7%	0.88
Freeman–Durden-based classification	90.3%	0.88
Yamaguchi based-classification	94.1%	0.93

classification (90.3%) and Cloude–Pottier-based classification (89.7%). Results show that the use of full polarimetric data improves the detection of structural differences between forest canopies, thus helping in better forest mapping and management practices. The new generation of full polarimetric SAR technology could help to study forest parameters for better implementation of REDD policies.

Acknowledgements

The authors are highly thankful to the Monbukagakusho (MEXT) Japanese Government Fellowship to pursue research at The University of Tokyo, Japan. Authors also want to emphasize the contribution of the Institute of Industrial Science, The University of Tokyo for facilitating data analysis in its laboratories and also to the Department of Civil Engineering, The University of Tokyo for providing funds during the field visits. We would like to thank the Forestry Administration (FA), Cambodia for their cooperation during the field data collection.

Notes on contributors

Ram Avtar received the M.Sc. and M.Phil. degree in environmental science from Jawaharlal Nehru University, New Delhi, India. Presently he is a doctoral student of Department of Civil Engineering, The University of Tokyo, Japan. His doctoral research is focused on multi-sensor remote sensing techniques for forest management practices in Cambodia for effective implementation of REDD+ policies.

Wataru Takeuchi is an associate professor at the University of Tokyo. His main research is focused on remote sensing applications on environment and disaster assessment from local to global level.

Haruo Sawada is a professor at the University of Tokyo. His main research interest is the use of remote sensing in forestry and disaster management form local to global level.

References

- Ainsworth, T.L., Kelly, J.P., and Lee, J.S., 2009. Classification comparisons between dual-pol, compact polarimetric and quad-pol SAR imagery. *ISPRS Journal of Photogrammetry and Remote Sensing*, 64, 464–471.
- Alberga, V., 2007. A study of land cover classification using polarimetric SAR parameters. *International Journal of Remote Sensing*, 28 (17), 3851–3870.
- An, W., et al., 2011. Four-component decomposition of polarimetric SAR images with deorientation. *IEEE Transactions on Geoscience and Remote Sensing*, 8(5), 1–5.
- Asner, P.G., 2009. Tropical forest carbon assessment: integrating satellite and airborne mapping approaches. *Environment Research Letter*, 4, 1–11.
- Brown, S., 2002. Measuring carbon in forests: current status and future challenges. *Environmental Pollution*, 116, 363–372.

- Cloude, S.R. and Pottier, E., 1996. A review of target decomposition theorems in radar polarimetry. *IEEE Transactions on Geoscience and Remote Sensing*, 34 (2), 498–518.
- Cloude, S.R. and Pottier, E., 1997. An entropy based classification scheme for land applications of polarimetric SAR. *IEEE Transaction on Geoscience and Remote Sensing*, 35, 68–78.
- Congalton, R.G., 1991. A review of assessing the accuracy of classification of remote sensing data. *Remote Sensing of Environment*, 37, 35–46.
- Defries, R. et al., 2007. Earth observations for estimating greenhouse gas emissions from deforestation in developing countries. *Environmental Science & Policy*, 10, 385–394.
- Fang, C. and Wen, H., 2005. A new classification method based on Cloude Pottier eigenvalue/eigenvector decomposition. In: *IEEE International Geoscience and Remote Sensing Symposium Proceedings, IGARSS 2005*, 25–29 July 2005, Seoul, Korea, 1–5.
- Fang, C., Wen, H., and Yirong, W., 2006. An improved Cloude-Pottier decomposition using H/α/SPAN and complex Wishart classifier for polarimetric SAR classification. *CIE 06, International conference on Radar*, Shanghai.
- FAO, 2005. *Global forest resources assessment, food and agriculture organisation of the United Nations*. Rome.
- Ferro-Famil, L., Pottier, E., and Lee, J.S., 2001. Unsupervised classification of multifrequency and fully polarimetric SAR images based on the H/A/Alpha Wishart classifier. *IEEE Transactions on Geoscience and Remote Sensing*, 39 (11), 2332–2342.
- FRA, 2010. *Global forest resources assessment, food and agriculture organisation of the United Nations*. Rome.
- Freeman, A. and Durden, S.L., 1998. A three-component scattering model for polarimetric SAR data. *IEEE Transactions on Geoscience and Remote Sensing*, 36, 963–973.
- Garcia-Mora, T.J., Mas, J., and Hinkley, E.A., 2011. Land cover mapping applications with MODIS: a literature review. *International Journal of Digital Earth*, DOI: 10.1080/17538947.2011.565080.
- Gaughan, A.E., Binford, M.W., and Southworth, J., 2009. Tourism, forest conversion, and land transformations in the Angkor basin, Cambodia. *Applied Geography*, 29, 212–223.
- Ince, T., 2010. Unsupervised classification of polarimetric SAR image with dynamic clustering: an image processing approach. *Advances in Engineering Software*, 41, 636–646.
- Kohavi, R. and Provost, F., 1998. Glossary of terms in: editorial for the issue on applications of machine learning and the knowledge discovery process. *Machine Learning*, 30, 2–3.
- Kummer, D.M. and Turner, B.L., 1994. The human causes of deforestation in Southeast Asia. *Bioscience*, 44 (5), 323–326.
- Lee, J.S., Ainsworth, T.L., and Chen, K., 2008. Speckle filtering of dual polarization and polarimetric SAR data based on improved sigma filter. *IEEE IGARSS*, IV, 21–24.
- Lee, J.S. and Pottier, E., 2009. *Polarimetric radar imaging: from basics to application*. Boca Raton: CRC Press, Taylor and Francis Group.
- Lee, J.S., et al., 1999. Unsupervised classification using polarimetric decomposition and the complex Wishart classification. *IEEE Transactions on Geoscience and Remote Sensing*, 37 (5), 2249–2258.
- Lee, J.S., et al., 2004. Unsupervised terrain classification preserving polarimetric scattering characteristics. *IEEE Transactions on Geoscience and Remote Sensing*, 42 (4), 722–731.
- Lee, J.S., et al., 2009. Improved sigma filter for speckle filtering of SAR imagery. *IEEE Transactions on Geoscience and Remote Sensing*, 47 (1), 202–213.
- Lu, D. and Weng, Q., 2004. Spectral mixture analysis of the urban landscapes in Indianapolis with Landsat ETM+ imagery. *Photogrammetric Engineering & Remote Sensing*, 70 (1), 1053–1062.
- Lu, D., 2006. The potential and challenge of remote sensing-based biomass estimation. *International Journal of Remote Sensing*, 27 (7), 1297–1328.
- Ouarzeddine, M., et al., 2005. Polarimetric classification using the Cloude/Pottier decomposition. *PolinSAR 2005*.
- Palmann, C., et al., 2008. Earth observation using radar data: an overview of applications and challenges. *International Journal of Digital Earth*, 1, 171–195.

- Patel, P., Srivastava, H.S., and Navalgund, R.R., 2009. Use of synthetic aperture radar polarimetry to characterize wetland targets of Keoladeo National Park, Bharatpur, India. *Current Science*, 97 (4), (25), 529–537.
- Pottier, E., 1998. Unsupervised classification scheme and topography derivation of PolSAR data based on the H/ α /A polarimetric decomposition theorem. *International workshop on Radar polarimetry*, France, 535–548.
- Pottier, E., Ferro-Famil, and Lee, J.S., 2008. *POLSARPRO V4.0 – lecture notes: advanced concepts*. [online]. Available at: <http://www.earth.esa.int/polsarpro/> [Accessed 21 August 2009].
- Rignot, E., Zimmermann, R., and Zyl van, J., 1995. Spaceborne applications of P band imaging radars for measuring forest biomass. *IEEE Transactions on Geoscience and Remote Sensing*, 33 (5), 1162–1165.
- Schlamadinger, B. and Marland, G., 1996. The role of forest and bioenergy strategies in the global carbon cycle. *Biomass and Bioenergy*, 10 (5/6), 275–300.
- Singh, G., Yamaguchi, Y., and Park, S.E., 2011. Utilization of four component scattering poser decomposition method for glaciated terrain classification. *Geocarto International*.
- Trisasongko, B.H., 2010. The use of polarimetric SAR data for forest disturbance monitoring. *Sensing and Imaging*, 11, 1–13.
- UNEP, 2009. *Cambodia environment outlook*. Report published by Ministry of Environment, Kingdom of Cambodia.
- Wang, H., Huang, Q., and Pi, Y., 2009. Polarization decomposition with S and T matrix of a PolSAR image. *ICCCAS 2009*.
- Yamaguchi, Y., *et al.*, 2005. Four-component scattering model for polarimetric SAR image decomposition. *IEEE Transaction on Geoscience Remote Sensing*, 43 (8), 1699–1706.
- Yamaguchi, Y., Yajima, Y., and Yamada, H., 2006. A four-component decomposition of POLSAR images based on the coherency matrix. *IEEE Geoscience and Remote Sensing Letter*, 3, 292–296.
- Zebker, H.A., *et al.*, 1991. Calibrated imaging radar polarimetry: technique, examples, and applications. *IEEE Transaction on Geoscience and Remote Sensing*, 29 (6), 942–961.